



Contents lists available at ScienceDirect

Arabian Journal of Chemistry

journal homepage: www.sciencedirect.com

Original article

Molecular mechanics and dynamics simulation of CD-47/SIRP α blockade study: A computational study on overcoming immunotherapeutic resistance in pancreatic ductal adenocarcinoma



Oluwatosin A. Saibu^{a,*}, Temitope M. Ajayi^b, Damilola A. Omoboyowa^c, Oladapo O. Oladipo^d, Sodiq O. Hammed^{d,e}, Tope T. Odunitan^{b,e}, Adenrele T. Oluwafemi^b, Aderonke J. Adejuyigbe^d, Gideon O. Aloba^b, Toheeb A. Balogun^c, Abdullahi O. Alausa^g, Damilola S. Bodun^c

^a Department of Chemistry and Biochemistry, New Mexico State University, Las Cruces, USA

^b Department of Biochemistry, Ladoko Akintola University of Technology, Ogbomoso, Oyo State, Nigeria

^c Phyto-medicine and Computational Biology Lab, Department of Biochemistry, Adekunle Ajasin University, Akungba-Akoko, Ondo State, Nigeria

^d Department of Physiology, Ladoko Akintola University of Technology, Ogbomoso, Oyo State, Nigeria

^e Genomics Unit, Helix Biogen Institute, Ogbomoso, Oyo State, Nigeria

^f Biological and Pharmaceutical Laboratory, Department of Chemical and Biochemical Engineering, University of Iowa, USA

ARTICLE INFO

Article history:

Received 22 November 2022

Accepted 10 September 2023

Available online 15 September 2023

Keywords:

PDAC

CD47

SIRP α

ADME

In silico

Immunotherapeutic

ABSTRACT

The sting of pancreatic ductal adenocarcinoma remains an irksome burden to the human populace. The focus of recent research has switched from finding the perfect medicinal medication to blocking immunological checkpoint proteins such as the signal regulating protein alpha-cluster of differentiation 47 (SIRP α -CD47). The search for CD47/SIRP α inhibitors with excellent oral bioavailability and permeability continues to elude researchers. This research aims to identify bioactive molecules with negligible side as inhibitor SIRP α -CD47 signaling cascade. Bioactive flavonoids from African medicinal plants were virtually screened against the SIRP- α binding site of CD47 using Schrodinger suite 2017-v1. The docking score was validated and complex stability performed using Gromacs. Among the bioactive flavonoids, five (5) compounds were predicted as potent inhibitors of CD47 with pelargonidin observed to have the best binding affinity of -6.715 kcal/mol. Validation using QSAR and pharmacophore modeling further confirm the interaction with predicted pIC50 range of 5.981 to 6.841 μ M and fitness score of 1.109 to 1.530. Drug-likeness prediction revealed that all hit compounds obey Lipinski's rule of five. The MD simulation result predicted the stability of pelargonidin and malvidin comparable to the standard drug NCGC00138783. The quantum mechanics estimation revealed that, the hit compounds have proton donating and accepting ability hence, they possess inhibitory potential. From the molecular docking, post-docking and MD simulation analyzes of this study, Pelargonidin, malvidin and Peonidin were proposed as suitable candidates that could be probed further for developing a new target-specific immunotherapeutic agent against PDAC.

© 2023 Published by Elsevier B.V. on behalf of King Saud University. This is an open access article under the CC BY-NC-ND license (<http://creativecommons.org/licenses/by-nc-nd/4.0/>).

* Corresponding author.

E-mail address: saioluwatosin@gmail.com (O.A. Saibu).

Peer review under responsibility of King Saud University.



<https://doi.org/10.1016/j.arabjc.2023.105265>

1878-5352/© 2023 Published by Elsevier B.V. on behalf of King Saud University.

This is an open access article under the CC BY-NC-ND license (<http://creativecommons.org/licenses/by-nc-nd/4.0/>).

1. Introduction

Over the past ten years, cancer has remained one of the top causes of death despite extensive study and rapid advancement (Sandeep and Sobhia, 2018). Pancreatic ductal adenocarcinoma (PDAC) was described by World Health Organization as one of the most prevalent and fatal types of cancer and one of the contributors to this unpleasant burden (Da-Costa et al., 2020). The increase in recently identified cases of pancreatic ductal adenocarcinoma is still a topic of discussion in cancer research. The cure remains elusive, and multiple attempts at developing the optimum

treatment for PDAC, a disease with low survival, have been unsuccessful (Beatty et al., 2017). As a result, research has shifted toward immunotherapy. Immunotherapy is a cancer treatment strategy that takes advantage of the immune system's specificity and heterogeneity (Yang, 2015). Unfortunately, PDAC has resisted immunotherapy, varying from small molecule antibodies to viral modifications during treatment and various alterations in its signaling pathway could explain the reasons behind resistance mechanisms (Alausa et al., 2022). The limitation of cytotoxic T-cell responses to cancer cells is distinguishing trait cancers developed to evade host immunological responses. To treat and manage various malignancies, immunotherapeutic research has recently moved its focus to block checkpoint proteins such as PD-1, CTLA-4, LAG3, TIM3, TIGIT, and BTLA (Sarantis et al., 2020). In healthy conditions, immune checkpoint proteins regulate immune response by limiting autoimmunity. However, they hinder cytotoxic T-cell activity in cancer by inhibiting interactions between T-cells and antigen-presenting cells or malignant cells (Sharma and Allison, 2015).

Since its emergence in the late 1990s, the SIRP α -CD47 checkpoint has been demonstrated to be essential for cancer immune evasion (Jiang et al., 1999; Logtenberg et al., 2019). Fig. 1 showed the crystal structure of the CD47 with the red, green, grey and blue colours representing the N-terminal amino acids, C-terminal amino acids, α -helices and β -fold sheets respectively.

All human cells express the *trans*-membrane protein CD-47, but specific tumour cells have high levels of this protein (Zola et al., 2020). It is a cell surface glycoprotein related to the immunoglobulin superfamily that binds to several different proteins, including signal regulatory protein (SIRP), thrombospondin 1, and integrin (Zola et al., 2020). Numerous cancers rely on the tumour antigen CD47 for growth and spread. The focus of research has been on creating therapeutic drugs that significantly disrupt the SIRP α -CD47 signalling cascade. This cascade prevents dendritic cells from phagocytosing tumours, deactivating innate immunity, and ultimately leading to tumour regression (Alausa et al., 2022). Phagocytosis is inhibited by the interaction of CD47 with SIRP α , which sends the macrophages a "don't eat me" signal (Brown and Frazier, 2001). As a result, tumour cells might avoid immune monitoring by the inhibition of phagocytic processes when CD47 is overexpressed. It takes more than only CD47 inhibition to activate



Fig. 1. Crystal structure of CD47.

macrophage anti-tumour action. Recent studies indicated that the CD47-SIRP α axis, like the PD-1/PD-L1 in solid tumours is an essential immune checkpoint in various cancers.

Traditional medicine has a rich history of using natural substances to treat cancer. Additionally, about 60% of current anti-cancer therapeutics was derived from natural products and medicinal plants (Takahashi, 2018). Hence, this research focuses on discovering natural compounds capable of alleviating immunotherapeutic resistance in PDAC by targeting the CD47 using computational molecular mechanics, molecular dynamics, and quantum investigations.

2. Methods

The E-pharmacophore hypothesis development and screening, virtual screening, MM-GBSA calculation and QSAR modeling were performed using Maestro Schrodinger 2017v1 software. The ADME analysis was performed using web server, quantum calculation was carried out using Spartan 14 software and MD simulation by Gromacs. All computational studies were performed on a Dell computer with a Windows-10 OS, an Intel core i3 processor, and 8 GB RAM.

2.1. Protein preparation

The three-dimensional X-ray crystallographic structure of a complex of human signal regulatory protein SIRP α complex with CD47 (PDB ID: 2JJS) was chosen. The protein was prepared using the Schrodinger suite's protein preparation package. The preparation included the assignment of hydrogen bonds, bond orders, hydrogen addition, optimization, protein minimization, removal of all chains excluding chain C (CD47 chain), and deletion of waters (Newman et al., 2003).

2.2. Grid generation

The receptor grid was created using the amino acids found on the surface of CD47 that are important for binding to SIRP α (Sandeep and Sobhia, 2018). GLU 35, THR 99, ARG 103, GLU 97, THR 102, GLU 100, GLU 104, LEU 101 and GLU 106 are among the amino residues. The coordinates for the X, Y, and Z axis are 28.98, -14.73, and 35.32 respectively.

2.3. Ligand preparation

Flavonoids with cancer-inhibitory properties from medicinal plants were retrieved from literature. The flavonoids' three-dimensional structure was downloaded in Sdf format from Pubchem database. The compounds were prepared with the Maestro Schrodinger software's LigPrep module. Fig. 2 shows the initially screened top ranking ligand structures as well as their chemical names.

2.4. Structure-based screening

GLIDE structure-based screening includes three precision methods: HTVS, standard precision (SP) docking, and XP docking. This study used two docking precisions to obtain a potential lead molecule quickly. HTVS can swiftly screen a vast number of molecules; however, the sampling techniques were constrained, making it difficult to interpret the results. As a result, SP was used to dock all the ligands (16) with high glide score from the HTVS precision analysis, which chooses an appropriate binding pose from a broad pool of ligands.

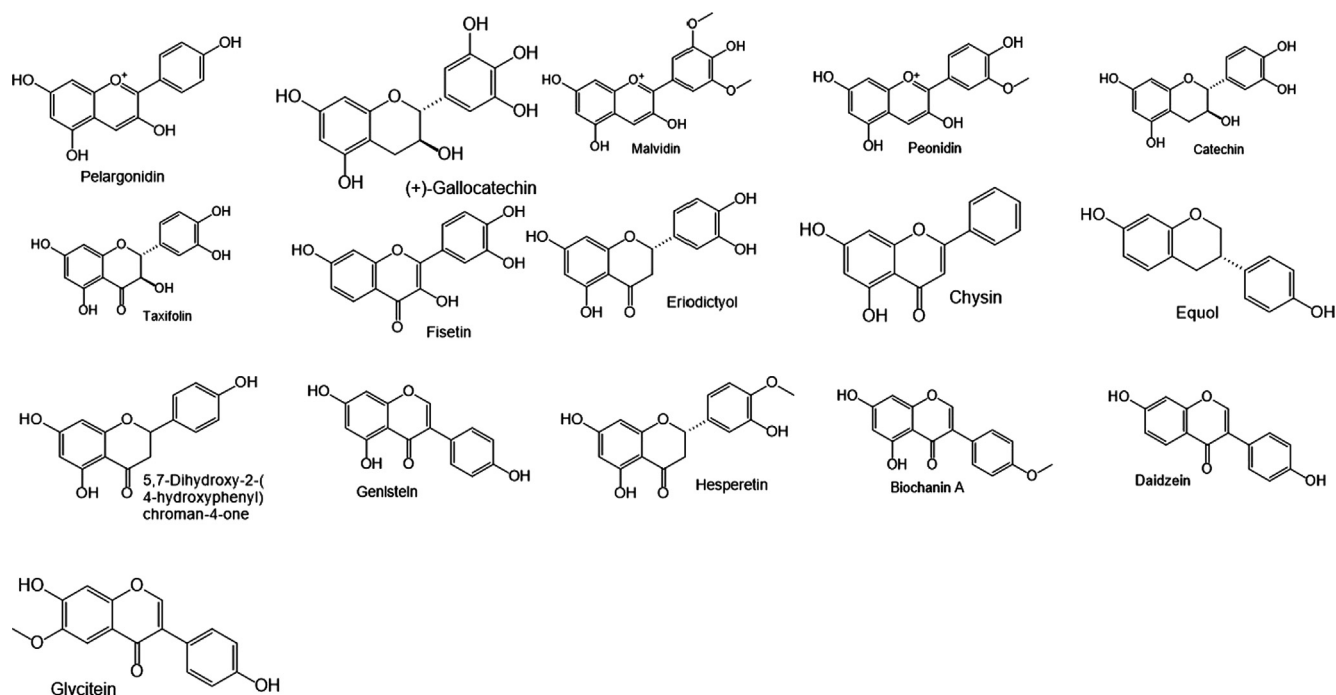


Fig. 2. 2D Structure and name of the selected flavonoids.

2.5. Generation of pharmacophore hypothesis

The standard drug (NCGC00138783) was used to generate an energy optimized pharmacophore model for the crystal structure of CD47. The model was generated from protein-ligand option of the phase develop pharmacophore tool of schrodinger suite (2017–1) (Omoboyowa et al., 2023). The pharmacophore model is shown in Fig. 3.

The virtual screening base on E-pharmacophore was performed with the five (5) flavonoids with top docking scores after preparation using macro model minimization. The pharmacophore-based analysis was carried out with phase module to generate a subset of molecules having chemical features for binding to CD47 according to the generated model. The fitness scores were used to justify the best hits.

2.6. Development of automated QSAR model

By blasting the FASTA sequence of the protein received from PDB, the protein inhibitors with their corresponding IC₅₀ were extracted from the ChEMBL database (<https://www.ebi.ac.uk/chembl/>) with the chain C (CD47 chain) sequence (shown below) used for the blasting. The inhibitory chemicals were translated to sdf format using the Data-Warrior software (v.2) (Omoboyowa et al., 2022). The sdf format of the inhibitors was imported into the Schrodinger suite workspace and prepared using the macro model minimization tool. The QSAR model for the protein was developed. The best-projected rank was kpls molprint 24, with the model's prediction precision measured by the ranking score, RMSE, SD, Q₂, and R₂. The pIC₅₀ of a lead compound was predicted using this approach.

2.7. CD47 FASTA sequence for ChEMBL blast

>2JJS_2|Chains C|LEUKOCYTE SURFACE ANTIGEN CD47|HOMO SAPIENS (9606).

```
QLLFNKTKSVEFTFGNDTVVIPCFVTNMEAQNTTEVYVKWKFKGRDI
YTFDGLNKTSTVPTDFSSAKIEVSQLKGDASLKMDSKSDAVSHTGNYTC
EVELTREGETIIEELKYRVVSWSTRHHHHHHH.
```

2.8. Free binding energy calculation (MM-GBSA)

The docking results showed that the selected ligands bind to the protein's active site via the receptor grid. However, it was unclear if this binding would be sufficient to cause a biological response as this depends primarily on the free binding energies of the protein–ligand complex. The binding free strengths of the top-ranking compounds and the reference drug were determined using the MM-GBSA module of the Schrodinger software.

2.9. Quantum chemical methods

Theoretical calculations have been widely studied through a powerful tool denoted as the Density Functional Theory method (DFT) due to its structural and spectral explanation of organic molecules. All calculations were performed and computed by spartan 14 software by wavefunction Inc on the top five hit compounds. The study was carried out with complete optimization of all geometrical variables via 6-31G* basis set, and this was accomplished with B3LYP density functionals (Huang et al., 2021). Frontier molecular orbitals (FMOs) energy was calculated, i.e., for the top five hit compounds identified, which by calculation deduce the energy band gap (Eq (1), which according to Koopman's theorem, predicts the interacting center.

$$E_g = E_{LUMO} - E_{HOMO} \quad (1)$$

2.10. Insilco ADMET prediction

We were interested in the drug-likeness properties of the top five hits identified through molecular docking. This was accomplished with the help of the QikProp module. Then, additional ADME properties were obtained from the online web server

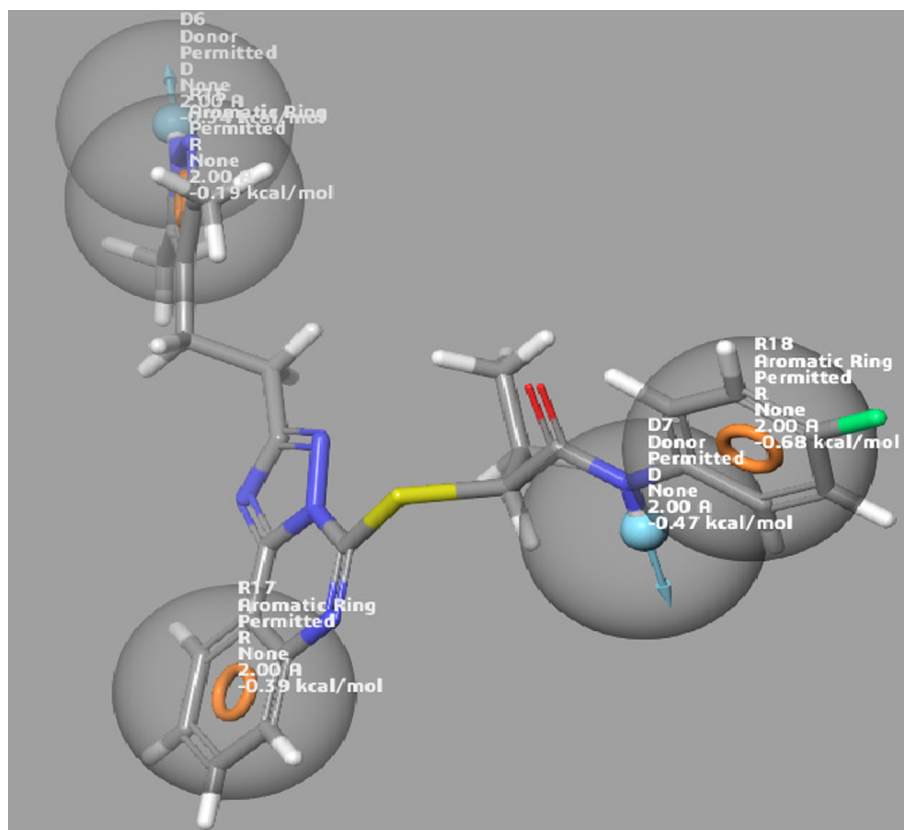


Fig. 3. The pharmacophore hypothesis generated with the standard drug.

AdmetSar (<https://lmm.d.ecust.edu.cn/>). The ligands' chemical structures were provided. The structures were translated to their canonical simplified molecular-input line-entry system (SMILE) to determine the ligand's physicochemical properties and pharmacokinetic models (Jensen, 2001). The drug-likeness of can be used to establish if a ligand is suitable for oral administration. The *in silico* prediction is based on Lipinski's rules (molecular weight, hydrogen bond donor, and hydrogen bond acceptor) (Cheng et al., 2012).

2.11. Molecular dynamic (MD) simulation

After the docking screening, the top ligand–protein complexes were further submitted to molecular dynamics simulation. Other approaches are needed for validation because the dynamics of the complexes were not considered during the molecular docking procedure. Using molecular dynamic simulations, the stability of docked Protein-Ligand complexes was evaluated. LiGRO (Yao et al., 2017) was used to set up the simulation system, and a

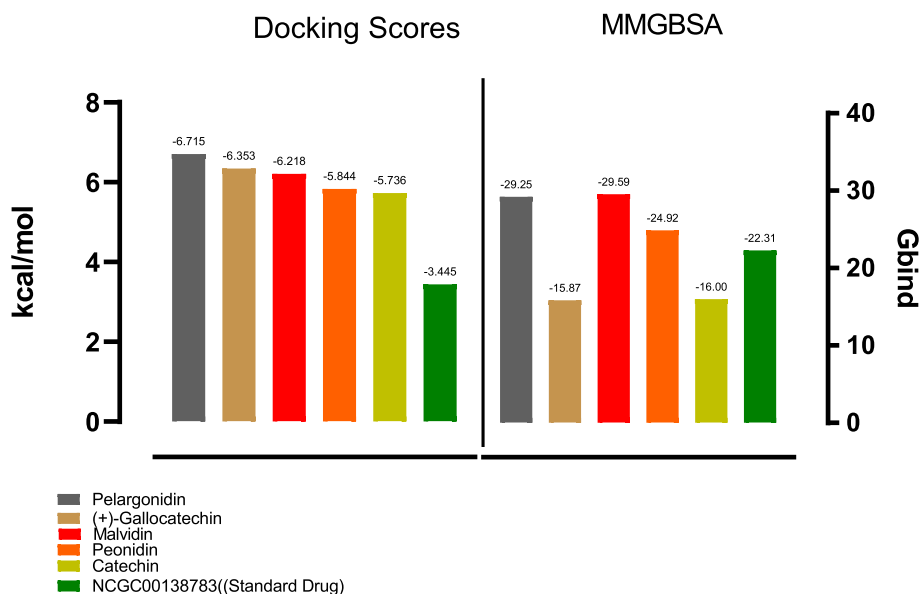


Fig. 4. Graph depicting the docking and MM-GBSA scores for the top five hits including the standard drug.

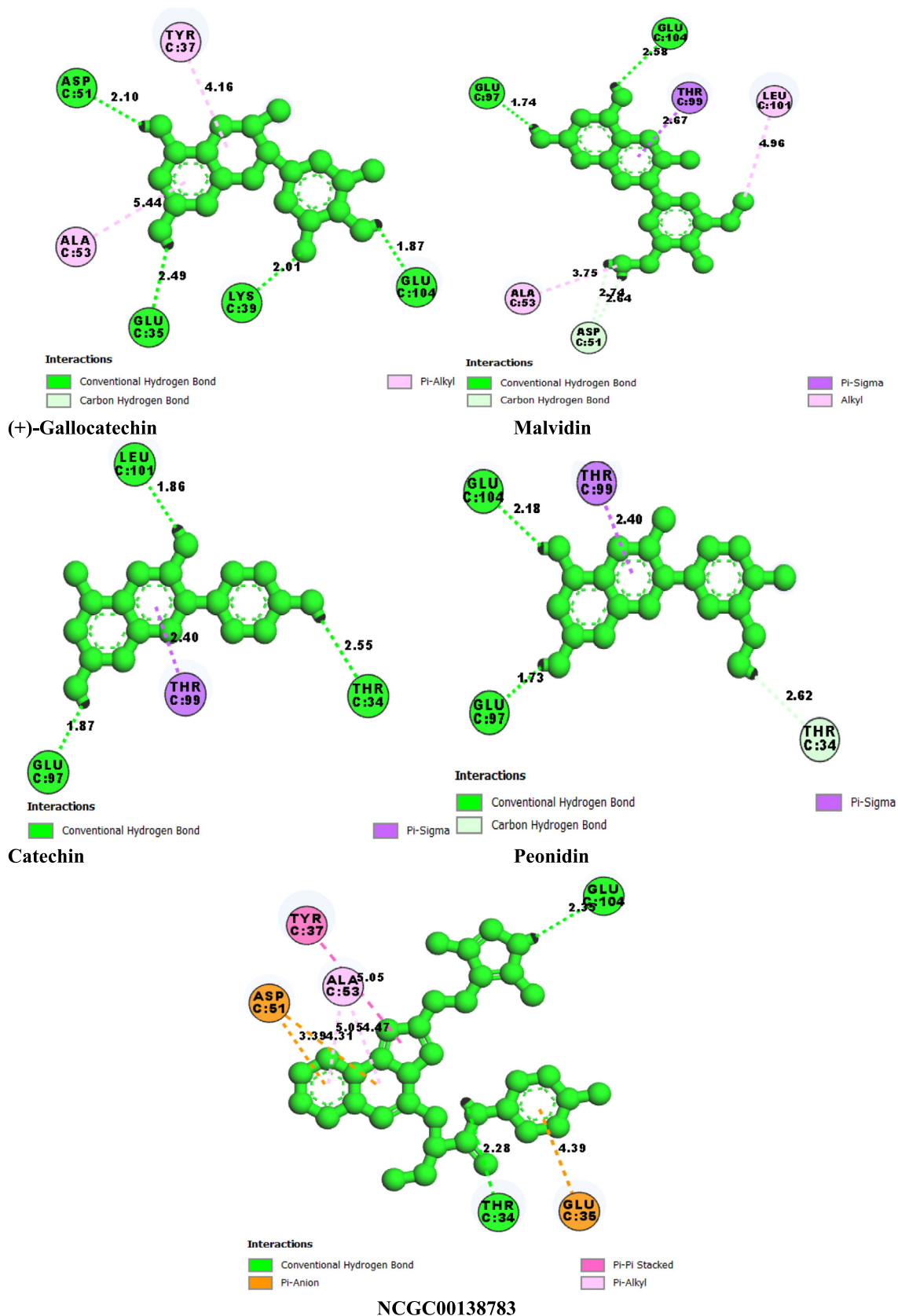


Fig. 5. 2D molecular interaction SIRP α binding pocket with hit compounds. (a) Pelargonidin (b) (+)-Galocatechin (c) Malvidin (d) Peonidin (e) Catechin (f) NCGC00138783 (Standard Drug).

GUI-based tool produced the system file needed to execute the simulation. The target was dissolved in a cubic box filled with TIP3P molecules of water with 150 mM NaCl ion concentration. The target was parameterized using the Amber99sb force field, and the ligand molecules were parameterized using LiGRO's ACPYPE module. The study by Omoboyowa et al. served as the guide for preparing all other simulation systems and parameters. GROMACS 5.1.5 was used to generate a run for each complex system that lasted 100 ns (Omoboyowa et al., 2022).

2.12. MD simulation trajectories analysis

Using conventional GROMACS tools, the trajectories of the MD simulation were evaluated for the root mean square fluctuation, radius of gyration (RG), H-bond mapping and root mean square deviation. The generated trajectories were shown in the PyMOL visualization graphics system (Version 2.0 Schrödinger, LLC.). Using the Molecular-dynamics-Interaction-plot tool, the interaction proportions of the target residues interacting with the compounds were computed (Jiang et al., 2021).

3. Results and discussion

3.1. Molecular docking, MMGBSA and interaction profiling

The protein CD47 was docked by the selected flavonoid derivatives to predict binding energy and interaction with the protein. Before docking was carried out, the protein was analyzed for its residues, which were vital for interacting with its partner protein CD-47.

Pelargonidin and (+)-Gallicocatechin exhibited the highest binding energies of -6.715 kcal/mol and -6.353 kcal/mol respectively

compared to the standard drug, which has a binding energy of -3.445 kcal/mol (Fig. 4). Thus, the docking results were analyzed, and it was finally reported that among the top flavonoid compounds, Pelargonidin and (+)-Gallicocatechin exhibit the best binding interaction, essential in identifying and developing new therapeutics targeting CD47. This will block its interaction with CD47 as a strategy to prevent cancer. The 2D interaction diagram shows the residues involved in the ligand's binding (Fig. 5) and the 3D binding complexes were presented in Fig. 6. Pelargonidin, the top-ranked ligand, formed H-bonds with THR 34, GLU 97, LEU 101, and GLU 104. While the other ligands including the standard drug, interacted via H-Bond with GLU 104, a critical amino residue in the CD47 binding site. Malvidin and Peonidin had another unique interaction with TYR 37, called Pi-Cation. VAL 36, TYR 37, ALA 53, and LEU 101 were the same interacting hydrophobic amino acids in the top-ranked ligand and the standard drug. Additionally, all reported ligands, including the standard drug, have similar interactions with the following key hydrophobic amino acids: TYR 37, ALA 53, and LEU 101 as presented in Table 1. The formation of H-bond and other hydrophobic interactions between small molecules and the amino acid residues at the binding domain of the target is vital for their inhibitory potential (Omoboyowa, 2022). The Schrodinger suite's Prime module's MM-GBSA approach was used to calculate the binding energies of the top compounds with the highest docking scores. The lower the score, the higher the binding energy, this method provide a reliable statistical post-docking examination of docked complexes. The relative free binding energies of pelargonidin, (+)-gallicocatechin, malvidin, peonidin, and catechin are -29.25 , -15.87 , -29.59 , -24.92 , and -16.00 , respectively. Pelargonidin, Malvidin, and Peonidin exhibit higher binding energies than the reference drug, per the results of the MM-GBSA (-22.31).

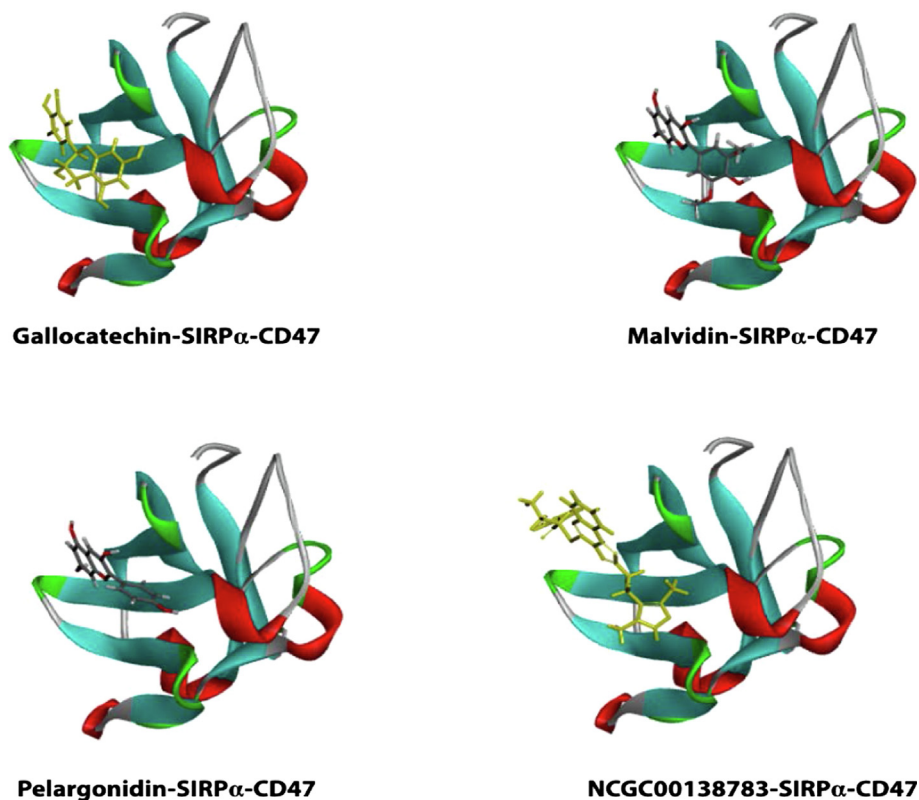


Fig. 6. 3D representation of hits with binding pocket of SIRP α .

Table 1
Interacting hydrophobic amino acids and H-Bond interacting amino acids for the top five hit compounds and standard drug.

Entry Name	H-Bond Residues	Hydrophobic Interacting amino acids	Other Interactions
Pelargonidin	LEU 101, GLU 104, GLU 97, THR 34	VAL 36, TYR 37, ALA 53, LEU 101	None
(+)-Gallocatechin	GLU 97, LYS 39, ASP 51, GLU 35, GLU 104	LEU 101, TYR 37, VAL 36, ALA 53	None
Malvidin	THR 34, LYS 39, GLU 97, LEU 101, GLU 104	ALA 53, TYR 37, LEU 101	Pi-Cation: TYR 37
Peonidin	ASP 51, LYS 39, GLU 104	ALA 53, VAL 36, TYR 37, LEU 101	Pi-Cation: TYR 37
Catechin	GLU 35, LYS 39, ASP 51, GLU 97, GLU 104	VAL 36, TYR 37, ALA 53, LEU 101	None
NCGC00138783(Standard Drug)	ASP 51, GLU 104	VAL 36, TYR 37, ALA 53, LEU 101	PI-PI STACKING: TYR 37

3.2. Virtual screening using E-pharmacophore model

Ligand-based pharmacophore approach is a vital computational model for drug design without macromolecular protein structure. This hypothesis is an ensemble of electronic and steric characters which are vital in ensuring molecular interactions with specific biological molecules and to stimulate or inhibit signaling pathways of such protein (Yang, 2010; Omoboyowa et al., 2023). In this study, Herein, the e-pharmacophore model was developed based on the standard drug-CD47 complex using four partitioning features. Fig. 3 showed the generated hypothesis with the standard

Table 2
E-pharmacophore fitness scores of lead compounds.

Entry Name	Fitness
Pelargonidin	1.185
(+)-Gallocatechin	1.109
Malvidin	1.191
Peonidin	1.143
Catechin	1.191
NCGC00138783(Standard Drug)	1.530

Table 3
The best model and Auto-QSAR parameters.

Model code	S.D	R ²	RMSE	Q ²
kpls_molprint2D_24	0.4354	0.8774	0.4220	0.8706

drug. The model with the best fitness score has one hydrogen bond acceptor, two hydrogen bond donors, one aromatic ring and hydrophobic interaction.

The fitness scores of the five (5) hits and standard drug are shown in Table 2. All the hit compounds showed fitness score greater than 1.0 with (+)-gallocatechin and catechin having the highest score of 1.191 followed by Catechin (1.531). Although the standard drug showed higher fitness scores higher (1.530).

3.3. Auto QSAR analysis

As it uncovers the correlations between the structural characteristics of chemical compounds and their biological activities, the quantitative structure–activity relationship (QSAR) is a computational model significant in drug development (Omoboyowa et al., 2023). AutoQSAR is a machine-learning approach that generates streams of independent variable-building models with various topological and physiochemical descriptors (Dixon et al., 2016). The autoQSAR model divides the test compounds into a 25% test and a 75% train set, as shown in Table 5. The best predictive model from the experimental data was determined using the based partial least-squares regression (kpls) analysis: kpls molprint2D 29. The model parameters resulted in a standard deviation (S.D.) of 0.4354, R² of 0.8774, RMSE of 0.4220, and Q² of 0.8706 (Table 3). The experimental compounds' model showed more training sets (blue colour) than the test set (red colour) as observed in the scatter plot in Fig. 7. The distribution of the test and train set in Fig. 7 was consistent with the distribution observed in Table 5. The QSAR model was use to obtain the pIC50 of the hit compounds shown in

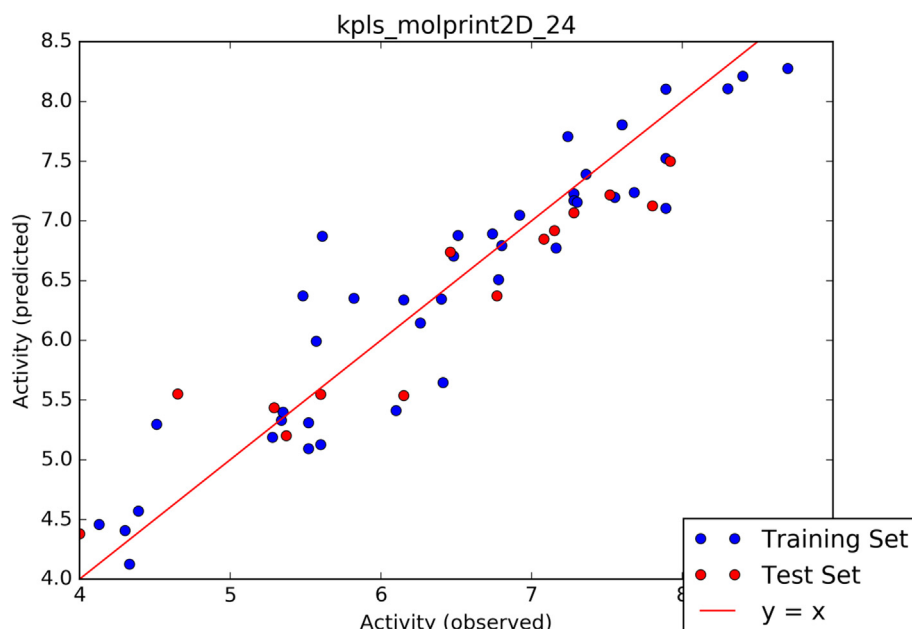
**Fig. 7.** Scatter plot of the best model.

Table 5, All the hit compounds and standard drug showed high pIC50 above 5.00 μM with pelargonidin and peonidin (6.001 μM) showing better pIC50 among the hit compounds comparable with the standard drug (6.841 μM). (See **Table 4**)

Table 4
Comparison with predicted and observed Auto-QSAR analysis.

ID	Set	pIC50 (observed)	pIC50 (predicted)	Residue error
1	Train	6.800	6.7053	0.2253
2	Train	7.2800	7.2276	-0.0524
3	Train	7.3600	7.3898	0.0298
4	Train	6.4100	5.6460	-0.7640
5	Train	6.7800	6.5088	-0.2712
6	Train	6.8000	6.7940	-0.0060
7	Train	4.3300	4.1273	-0.2027
8	Train	5.2800	5.1881	-0.0919
9	Train	7.8900	8.1051	0.2151
10	Train	5.5200	5.3111	-0.2089
11	Train	4.5100	5.2974	0.7874
12	Train	4.3900	4.5702	0.1802
13	Test	4.6500	5.5514	0.9014
14	Train	6.1500	6.3404	0.1904
15	Train	5.6100	6.8730	1.2630
16	Train	7.2800	7.1699	-0.1101
17	Train	6.5100	6.8792	0.3692
18	Train	7.2400	7.7064	0.4664
19	Train	6.7400	6.8927	0.1527
20	Train	4.3000	4.4081	0.1081
21	Train	6.4000	6.3470	-0.0530
22	Test	7.1500	6.9184	-0.2316
23	Test	4.0000	4.3802	0.3803
24	Train	7.6000	7.8038	0.2038
25	Train	7.5500	7.1972	-0.3528
26	Train	5.4800	6.3736	0.8926
27	Test	7.0800	6.8466	-0.2334
28	Test	6.4600	6.7386	0.2786
29	Train	5.5700	5.9920	0.4220
30	Train	7.8900	7.1059	-0.7841
31	Test	7.2800	7.0674	-0.2126
32	Train	7.3000	7.1560	-0.1440
33	Train	7.1600	6.7734	-0.3866
34	Test	5.2900	5.4361	0.1461
35	Train	7.8900	7.5223	-0.3677
36	Test	5.6000	5.5471	-0.0529
37	Test	7.8000	7.1266	-0.6734
38	Train	5.6000	5.1285	-0.4715
39	Train	6.1000	5.4129	-0.6871
40	Train	5.3400	5.3328	-0.0072
41	Train	5.3500	5.3987	0.0487
42	Test	7.5200	7.2172	-0.3028
43	Train	7.6800	7.2379	-0.4421
44	Train	8.7000	8.2774	-0.4226
45	Train	8.4000	8.2109	-0.1891
46	Train	7.6000	7.8038	0.2038
47	Train	6.9200	7.04796	0.1276
48	Train	5.8200	6.3538	0.5338
49	Test	5.3700	5.2028	-0.1672
50	Train	4.1300	4.4591	0.3291
51	Test	6.7700	6.3736	-0.3964
52	Train	8.3000	8.1063	-0.1937
53	Test	6.1500	5.5388	-0.6112
54	Test	7.9200	7.4993	-0.4207
55	Train	5.5200	5.0927	-0.4273
56	Train	6.2600	6.1460	-0.1140

Table 5
The best model and predicted pIC50 of lead compounds.

Pubchem ID	Compound Name	Predicted pIC50 (μM)
65,084	(+)-Galliccatechin	5.981
159,287	Malvidin	5.981
440,832	Pelargonidin	6.001
441,773	Peonidin	6.001
NCGC00138783	Reference Drug	6.841

3.4. Quantum calculations

The development of density functional theory (DFT) of small molecules is an important tool use to describe the molecular interactions between molecules and gives information concerning electron transfer within the molecule which is required to predict the chemical stability and reactivity of a molecule (Balogun et al., 2021). The energy of high occupied molecular orbital (E_{HOMO}) and low unoccupied molecular orbital (E_{LUMO}) and energy gap (Eg) estimated from the quantum mechanics calculations are vital in predicting molecular reactivity of bioactive compounds (Omoboyowa et al., 2023). From the results presented in table Fig. 8, the complete geometry optimization of the selected flavonoid derivatives at their low energy level, in which all analysis were computed on these least optimized flavonoid molecules.

From the results presented in Table 6 and Fig. 8, the electron donation potential of the hit compounds was suggested by the E_{HOMO} values which range from -5.63 to -9.25 eV and the electron accepting potential was predicted by the E_{LUMO} values which range from -6.12 to -0.08 eV. Hence, the high E_{HOMO} value and lower E_{LUMO} value are necessary for the predicted reactivity of the compounds. Energy gap (Eg) is the difference between the HOMO and LUMO energies and has been reported by Uzzaman and Mahmud (2020), as a predictor of the molecule stability and reactivity, higher value of Eg denote greater stability with less bioavailability and low reactivity (Omoboyowa et al., 2023). The Eg of the hits were estimated between the range of 2.56 to 5.71 eV suggesting that the hit compounds are reactive and stable molecules. (See Table 7 and Table 8.

3.5. Prediction of physicochemical and ADMET-TOX properties

The *in silico* drug-likeness predictions are founded on Lipinski's rule of five; hydrogen bond donor, hydrogen bond acceptor and molecular weight (Cheng et al., 2012). The druggability of a molecule is generally based on this rule. To ascertain if substances could penetrate the central nervous system, the blood-brain barrier penetration was evaluated (Table 5) (Karelson et al., 1996). Out of the five predicted molecules, only (+)-Galliccatechin and Catechin are likely to penetrate the blood-brain barrier. In humans, many cytochrome P450s catalyze the metabolism of various substances, including xenobiotics and medicines.

Thus, inhibition of cytochrome P450 isoforms may result in drug-drug interactions in which co-administered drugs fail to be metabolized and accumulate to toxic levels. The predicted compounds are CYP2D6 inhibitors and CYP2C9 substrates. All are predicted to be CYP3A4 substrates except for pelargonidin. Adverse drug administration-related effects are referred to as acute oral toxicity (Nyandoro, et al., 2018). Fortunately, all substances proved negative for acute toxicity and mutagenicity in the AMES test. Based on their acute oral toxicity, compounds are categorized into four classes. LD50 values for substances in Category I are less than or equal to 50 mg/kg. LD50 values for substances in Category II are higher than 50 mg/kg but lower than 500 mg/kg. LD50 values for substances in Category III are higher than 500 mg/kg but lower than 5000 mg/kg. The LD50 values of the substances in Category IV were higher than 5000 mg/kg. It is predicted that all the compounds will fall into Category III or IV. All of the compounds are thought to be non-carcinogenic. Drug solubility has previously been defined as a critical property of evaluating pharmaceuticals in the drug development cycle. This is because it helps to determine the concentration of the drug in the systemic circulation, resulting in a maximal optimal response (Walum, 1998). As a result of the presence of hydroxyl groups in the compounds, they were water-soluble. None of the substances is P-glycoprotein substrates (P-GB). The potassium channel, the human Ether-a-go-go

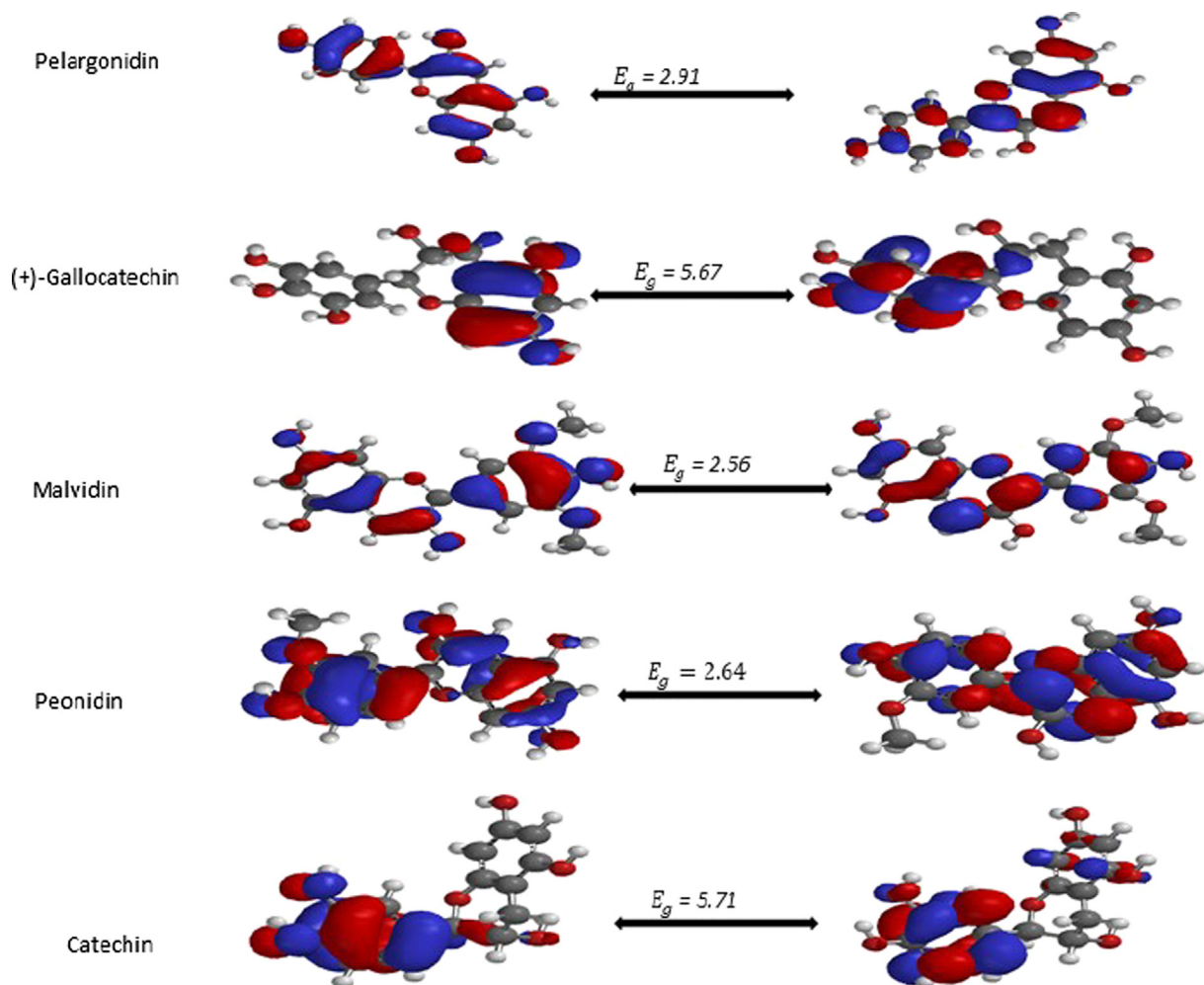


Fig. 8. HOMO and LUMO density for the five flavonoid derivatives.

Table 6
Quantum chemical reactivity parameters for the top five hit compounds.

Compounds	E_{HOMO}	E_{LUMO}	E_g
Pelargonidin	-9.25	-6.34	2.91
(+)-Gallocatechin	-5.65	0.02	5.67
Malvidin	-8.68	-6.12	2.56
Peonidin	-8.83	-6.19	2.64
Catechin	-5.63	0.08	5.71

Related Gene (hERG), is required for cardiac excitability control and regular heartbeat (Savjani et al., 2012). Since none of the chemicals inhibits the hERG gene, they cannot induce proarrhythmia. Pelargonidin, the lead compound, has been shown to have antioxidant properties after reducing oxidative markers. A research found the antioxidant efficacy of Pelargonidin via an increase in the level of the natural antioxidant enzymes catalase and superoxide

Table 7
Drug likeness properties of the standard and top five hit compounds.

Entry Name	mol MW	Hbond Acceptors	Hbond Donors	iLogP	Polar Surface Area	Rule of Five
Pelargonidin	271.24	5	4	-2.44	94.06	Suitable
(+)-Gallocatechin	306.27	7	6	1.47	130.61	Suitable
Malvidin	331.30	7	4	-1.96	112.52	Suitable
Peonidin	301.27	6	4	-1.94	103.29	Suitable
Catechin	290.27	6	5	1.33	110.38	Suitable
NCGC00138783(Standard Drug)	503.59	6	2	3.13	126.16	Suitable

dismutase (Lamothe et al., 2016; Mirshekar et al., 2010). The therapeutic potential of the screened compounds was determined using Christopher Lipinski's proposed rules of five (ROF) with a molecular weight of 500, HB donors of 5, HB acceptors of 10, and an octanol/water partition coefficient ($\log p$ 5) (Table 3) (Cheng et al., 2012). Except for gallocatechin, which possesses more than five HB donors, all the compounds met all the criteria.

3.6. Molecular dynamics simulation

Following the results generated from the molecular docking campaign, we employed the use of the following molecular dynamics parameters; RMSD, RMSF, HBOND and ROG in a 100 ns simulation to evaluate the dynamical stability of the three selected hit druglike candidates (Pelargonidin, (+)-Gallocatechin and Malvidin) and the reference drug (NCGC00138783). Their behavioral kinetics was also evaluated in both bound and unbound states with

Table 8
ADMET screening of the top hit compounds.

Model	Pelargonidin	(+)-Gallocatechin	Malvidin	Peonidin	Catechin
Ames mutagenesis	-	-	-	-	+
Acute Oral Toxicity (c)	III	IV	III	III	IV
Blood Brain Barrier	+	-	+	+	-
Caco-2	-	-	+	+	-
Carcinogenicity (binary)	-	-	-	-	-
CYP1A2 inhibition	-	-	+	+	-
CYP2C19 inhibition	-	-	+	+	-
CYP2C9 inhibition	-	-	+	+	-
CYP2C9 substrate	-	-	-	-	-
CYP2D6 inhibition	-	-	-	-	-
CYP2D6 substrate	-	+	-	-	+
CYP3A4 inhibition	-	-	+	+	-
CYP3A4 substrate	+	-	-	-	-
Hepatotoxicity	+	+	+	+	-
Human Ether-a-go-go-Related Gene inhibition	-	-	-	-	-
Human Intestinal Absorption	-	+	+	+	+
Human oral bioavailability	-	-	-	-	-
Acute Oral Toxicity	1.435115576	1.636945605	1.2353605	0.9769318	1.418269
P-glycoprotein inhibitor	-	-	+	-	-
P-glycoprotein substrate	-	-	-	-	-
PPAR gamma	+	+	+	+	+
Plasma protein binding	0.852887869	0.877940595	0.881655	0.9295143	0.987759
Subcellular localization	Nucleus	Mitochondria	Nucleus	Nucleus	Mitochondria
UGT catalyzed	-	+	+	+	+
Water solubility	-3.09788922	-3.101451725	-3.4489542	-3.343575	-3.101452

the protein structure (2JJS). Each complex was confined to an environment closely related to a normal physiological condition of a natural cell in terms of temperature, solvent, pressure, and ions throughout the simulation. To this end, we evaluated and compared the 100 ns spectrums of each prospective drug candidate complex against the reference drug (NCGC00138783).

3.7. Root mean square deviation

Using RMSD analysis, it is possible to determine the conformational and structural alterations of the backbone atoms of the protein-ligand entities (2JJS-NCGC00138783, 2JJS-GALLOCATECHIN, 2JJS-MALVIDIN, 2JJS-PELARGONIDIN and 2JJS). By comparison of RMSD spectrum of the referenced inhibitor and the unbound protein with the proposed hit compounds, one could speculate if the

binding of the chemical entities is stable and capable of binding stably at the binding pocket of the receptor (Roy et al., 2017). Hence, we calculated and plotted the RMSD of each simulated complex for the entire 100 ns MD production run (Fig. 9). Looking at the RMSD spectrum, Pelargonidin and Malvidin depicted almost the same graphical pattern with the standard compound throughout the entire simulation suggesting their potential to act as a putative binder of the protein target. This is evidenced with their close average RMSD of 0.1899 nm and 0.186 nm respectively, compared with the 0.175 nm of the referenced compound. In contrast, Gallocatechin showed a different RMSD pattern compared to the standard drug and the apoprotein (2JJS). However, with mean RMSD value of 0.30 nm, the ligand average RMSD value falls below 0.5 nm value which is acceptable for a considerable stable system (Adelusi et al., 2020). Overall, the RMSD result showed that the

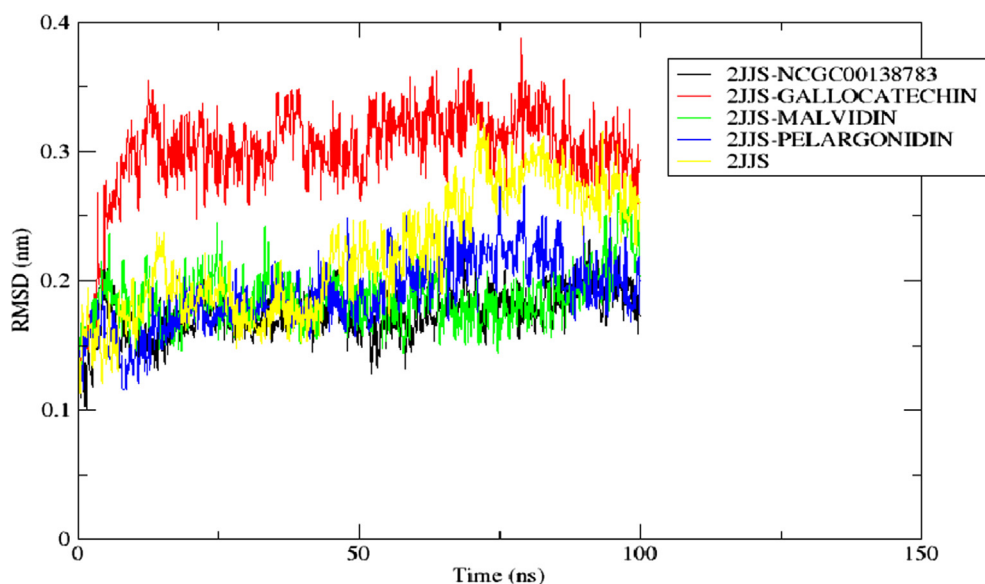


Fig. 9. The RMSD of the backbone atom of the protein in top docking scored hit complexes throughout 100 ns simulation.

binding of Malvidin, Pelargonidin, and Gallocatechin with the protein target are stable and suggest their ability to disrupt the SIRP α -CD47 signaling cascade.

3.8. Root mean square fluctuation of the top docking scored hit complexes

For examining the structural fluctuation of the amino acid residues of the bound and unbound complexes, as well as changes in the position of the ligand, the Root Mean Square Fluctuation (RMSF) is a commonly used metric. A higher average RMSF value denotes a system with more fluctuating residues while a lower average value corresponds to a system with less fluctuating residues (Roy et al., 2017). According to the result represented in Fig. 12, all the bounded system including the standard (2JJS-GALLOCATECHIN, 2JJS-MALVIDIN, 2JJS-PELARGONIDIN, and 2JJS-

NCGC00138783) demonstrate similar RMSF pattern. In comparison with the mean RMSF of the unbound receptor (0.199 nm), 2JJS-GALLOCATECHIN, 2JJS-MALVIDIN, 2JJS-PELARGONIDIN, and 2JJS-NCGC00138783, have lower average RMSF values of 0.146 nm, 0.135 nm, 0.152 nm, and 0.138 nm respectively. Interestingly, the RMSF result is consistent with the RMSD analysis which revealed that the binding of the ligands do not disrupt the conformational dynamics of the protein by depicting a lower average RMSD (with the exception of Gallocatechin) and RMSF values compared with the unbound form of the receptor (2JJS) (Fig. 10).

3.9. Hydrogen bond mapping of top docking scored hit complexes

Intermolecular H-bond is an important type of interaction that exists between protein–ligand complexes. Higher H-bond could be responsible for the greater stability of a compound at the binding

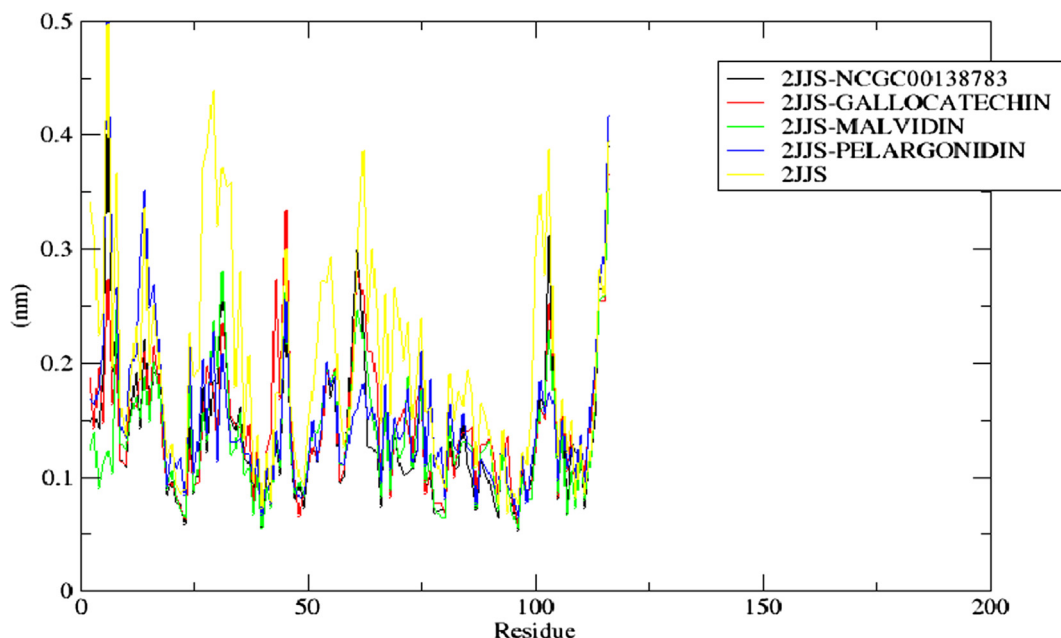


Fig. 10. The RMSF of the residues present in the protein (2JJS) of top docking scored hit complexes throughout the simulation period.

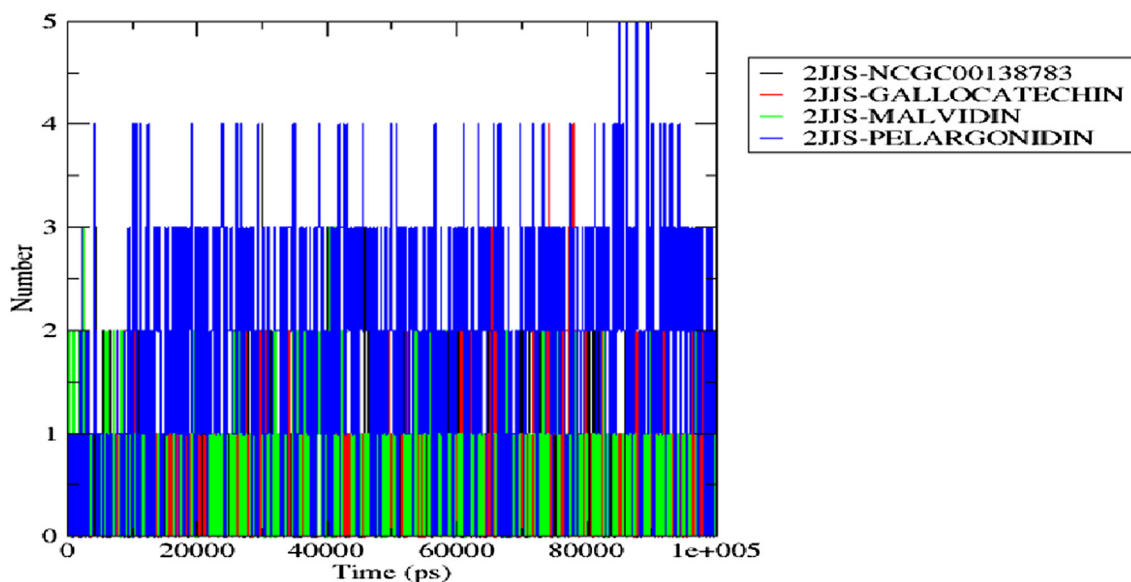


Fig. 11. H-bond distribution of the top docking scored hit complexes during 100 ns simulation run in the active site of the protein target.

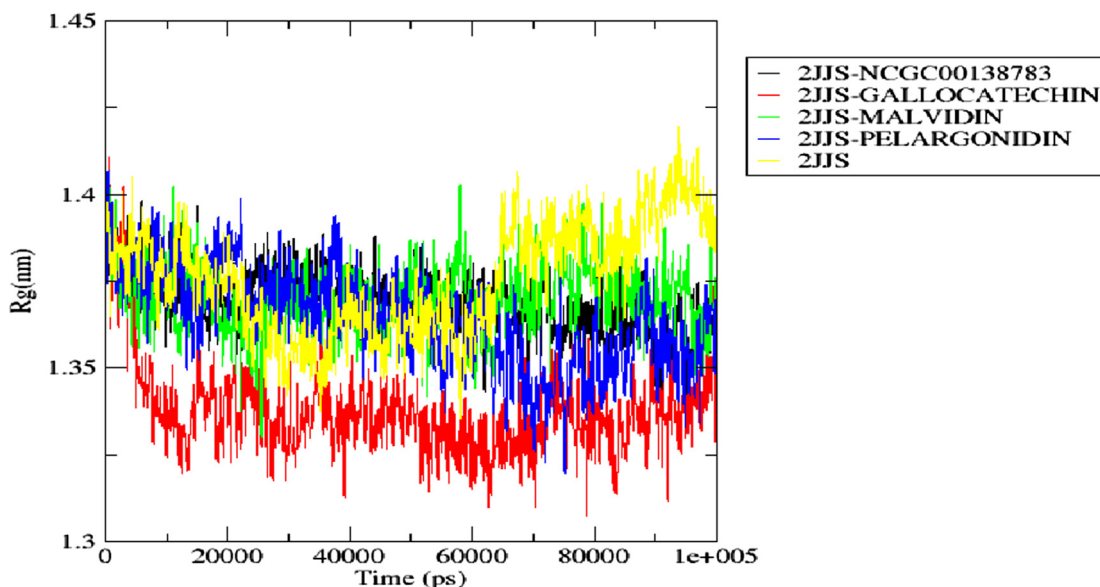


Fig. 12. Radius of gyration spectrum of the top docking scored hit complexes during 100 ns simulation run.

pocket of the receptor while lower H-bond may indicate a lower stable system (Lee et al., 2012). In the H-bond spectrum depicted in Fig. 11, Pelargonidin-one of the promising drug candidates showed thicker H-bond spectrum compared to all other binary complexes including the referenced inhibitor. Statistically, Pelargonidin, Malvidin, Gallocatechin, and the standard drug averaged 1.85, 0.44, 0.46, and 0.53 H-bonds respectively with their targeted receptor. Although Malvidin, and Gallocatechin have lower intermolecular H-bond, however, the difference between their values with the standard drug is not statistically significant and hence they could also be a good inhibitor of the protein using the H-bond metric.

3.10. Radius of gyration

The compactness of the secondary structures of the bound and unbound form of a simulated receptor is measured by radius of gyration (ROG). From this, one could determine if a system is stably folded or not. Fig. 12 shows the ROG plots of the apoprotein (2JJS) and the complexes (2JJS-NCGC00138783, 2JJS-Gallocatechin, 2JJS-Malvidin, 2JJS-Pelargonidin) as a function of time. Like the ROG result, Pelargonidin and Malvidin depicted similar ROG pattern with the standard drug throughout the entire simulation time. Their average ROG values are 1.364 nm, 1.370 nm, and 1.369 nm respectively. In contrast, Gallocatechin demonstrated different ROG pattern with the standard drug, but it has the lowest ROG value (1.337 nm) when compared with all other bounded systems. Our overall analysis of ROG indicates that the binding of the ligands does not distort the structural compactness of the receptor as they all averaged lower ROG values when compared with the apoprotein (1.376 nm) as shown in Fig. 12.

4. Conclusion

The interaction of CD47-SIRP α signaling allows cancer cells to elude immune detection and clearance by suppressing phagocytic action. As a result, this research aimed to predict a therapeutic drug that may circumvent immunotherapeutic resistance in PDAC

by suppressing SIRP α -CD47 signaling with minimal side effects in humans.

After computational analysis using molecular docking, molecular dynamics, and MM/GBSA quantum chemical calculations, the screened compounds (pelargonidin, malvidin, and peonidin) have higher binding energies than the reference medication. They also demonstrated better ideal stability and desirable intermolecular interactions in the selective pockets of CD47 compared to the reference medication (NCGC00138783). This study contributes to a better knowledge of the stability and interaction profile of protein–ligand complexes and the mechanism of inhibition involved in CD47–ligand complexes. According to the pharmacokinetic study, pelargonidin, malvidin and peonidin possess novel physicochemical characteristics and drug-like features. Additional in-vivo or in-vitro research is required to evaluate these ligands' pharmacological and biological activities in overcoming immunotherapeutic resistance in PDAC via CD47-SIRP α inhibition.

Author contributions

OAS conceived and designed the study. **TMA**, **DSB**, **OOO** and **SOH** contributed to the literature search; **ATO**, **AJA** and **GOA** contributed to data collection; **OAS**, **TMA** and **DAO** wrote the manuscript draft; **OAS** and **TMA** interpreted the results of the MD simulation; **TMA**, **OOO** and **ATO** contributed to the figures. **TAB**, **OAS**, **TMA**, **TTO**, and **AJA** contributed to editing and proofreading of the manuscript. **DAO** supervised the research. All authors agreed to the final manuscript.

Declaration of Competing Interest

The authors declare that they have no known competing financial interests or personal relationships that could have appeared to influence the work reported in this paper.

Acknowledgement

The authors wish to appreciate Olamide Olaoba (University of Missouri Columbia) for his insight during this study.

Appendix A. Supplementary material

Supplementary data to this article can be found online at <https://doi.org/10.1016/j.arabjc.2023.105265>.

References

- Adelusi, T.I., Oyedele, A.K., Boyenle, I.D., Ogunlana, A.T., Adeyemi, R.O., Ukachi, C.D., Idris, M.O., Olaoba, O.T., Adedotun, I.O., Kolawole, O.E., Xiaoxing, Y., Abdul-Hammed, M., 2020. Molecular modeling in drug discovery. *Inform. Med. Unlocked*. 24. <https://doi.org/10.1016/j.imu.2022.10088057> 100880.
- Alausa, A., Lawal, K.A., Babatunde, O.A., Obiwulu, E.N.O., Oladokun, O.C., Fadahunsi, O.S., Adegbola, P.I., 2022. Overcoming immunotherapeutic resistance in PDAC: SIRP α -CD47 blockade. *Pharmacol. Res.* 106264.
- Balogun, T.A., Ipinloju, N., Abdullateef, O.T., Moses, S.I., Omoboyowa, D.A., James, A. C., Saibu, O.A., Akinyemi, W.F., Oni, E.A., 2021. Computational evaluation of bioactive compounds from *Colocasia affinis* schott as a novel EGFR inhibitor for cancer treatment. *Cancer Inf.* 20, 1–12. <https://doi.org/10.1177/117693512111049>.
- Beatty, G.L., Eghbali, S., Kim, R., 2017. Deploying immunotherapy in pancreatic cancer: defining mechanisms of response and resistance. *Am. Soc. Clin. Oncol. Educ. Book* 37, 267–278. https://doi.org/10.1200/EDBK_175232.
- Brown, E.J., Frazier, W.A., 2001. Integrin-associated protein (CD47) and its ligands. *Trends Cell Biol.* 11, 130–135.
- Cheng, F., Li, W., Zhou, Y., Shen, J., Wu, Z., Liu, G., Lee, P.W., Tang, Y., 2012. AdmetSAR: a comprehensive source and free tool for assessment of chemical ADMET properties. *J. Chem. Information Model.* 52, 3099.
- da Costa Jr, W.L., Oluyomi, A.O., Thrift, A.P., 2020. Trends in the incidence of pancreatic adenocarcinoma in all 50 United states examined through an age period Cohort analysis. *JNCI Cancer Spectr.* 4 (4), 33.
- Dixon, S.L., Dian, J., Smith, E., Bargen, C.D., Sherman, W., Repasky, M.P., 2016. AutoQSAR: an automated machine learning tool for best-practice quantitative structural-activity relationship modeling. *Future Med. Chem.* 8 (15), 1825–1839.
- Huang, B., Bai, Z., Ye, X., Zhou, C., Xie, X., Zhong, Y., Lin, K., Ma, L., 2021. Structural analysis and binding sites of inhibitors targeting the CD47/SIRP α interaction in anticancer therapy. *Comput. Struct. Biotechnol. J.* 19, 5494–5503. <https://doi.org/10.1016/j.csbj.2021.09.036>.
- Jensen, F., 2001. Polarization consistent basis sets: Principles. *J. Chem. Phys.* 115, 9113–9125. <https://doi.org/10.1063/1.141524>.
- Jiang, P., Lagenaur, C.F., Narayanan, V., 1999. Integrin-associated protein is a ligand for the p84 neural adhesion molecule. *J. Biol. Chem.* 274, 559–562.
- Jiang, Z., Sun, H., Yu, J., Tian, W., Song, Y., 2021. Targeting CD47 for cancer immunotherapy. *J. Hematol. Oncol.* 14, 180. <https://doi.org/10.1186/s13045-021-01197-w>.
- Karelson, M., Lobanov, V.S., Katritzky, A.R., 1996. Quantum-chemical descriptors in QSAR/QSPR studies. *Chem. Rev.* 96, 1027–1043. <https://doi.org/10.1021/cr950202r>.
- Lamothe, S.M., Guo, J., Li, W., Yang, T., Zhang, S., 2016. The Human Ether-a-go-go-related Gene (hERG) potassium channel represents an unusual target for protease-mediated damage. *J. Biol. Chem.* 291, 20387–20401. <https://doi.org/10.1074/jbc.M116.743138>.
- Lee, G., 2012. Conformational sampling of flexible ligand-binding protein loops. *Bull. Kor. Chem. Soc.* 33, 770–774.
- Logtenberg, M.E.W., Jansen, J.H.M., Raaben, M., Toebes, M., Franke, K., Brandsma, A. M., 2019. Glutaminyl cyclase is an enzymatic modifier of the CD47-SIRP alpha axis and a target for cancer immunotherapy. *Nat. Med.* 61, 619.
- Mirshakar, M., Roghani, M., Khalili, M., Baluchnejadmojarad, T., Moazzen, S., 2010. Chronic oral pelargonidin alleviates streptozotocin-induced diabetic neuropathic hyperalgesia in rat: involvement of oxidative stress. *Iran. Biomed. J.* 14, 33–39.
- Newman, D.J., Cragg, G.M., Snader, K.M., 2003. Natural products as sources of new drugs over the period 1981–2002. *J. Nat. Prod.* 66, 1022–1037.
- Nyandoro, S.S., Shadrack, D., Munissi, J., Mubofu, E., 2018. In silico pharmacokinetic and molecular docking studies of N-cinnamoyltetraketide derivatives as inhibitors of cyclooxygenase-2 enzyme. *Tanzania J. Sci.* 44, 1–15.
- Omoboyowa, D.A., 2022. Exploring molecular docking with E-pharmacophore and QSAR models to predict potent inhibitors of 14- α -demethylase protease from *Moringa spp.* *Pharmacol. Res.- Mod. Chin. Med.* 4, 100147.
- Omoboyowa, D.A., Iqbal, M.N., Balogun, T.A., Bodun, D.S., Fatoki, J.O., Oyenehin, O.E., 2022. Inhibitory potential of phytochemicals from *Chromolaena odorata* L. against apoptosis signal-regulatory kinase 1: a computational model against colorectal cancer. *Comput. Toxicol.* 23. <https://doi.org/10.1016/j.comtox.2022.100235> 100235.
- Omoboyowa, D.A., Bodun, D.S., Saliu, J.A., 2023. Structure-based *in silico* investigation of antagonists of human ribonucleotide reductase from *Annona muricata*. *Inf. Med. Unlocked* 38, 101225.
- Roy, M., Pal, R., Chakraborti, A., 2017. Pelargonidin-PLGA nanoparticles: fabrication, characterization, and their effect on streptozotocin induced diabetic rats. *Indian J. Exp. Biol.* 55, 819–830.
- Sandeep, M., Sobhia, E., 2018. Design of anti-CD47 molecules using 1n silico approaches. *Br. J. Pharm. Med. Res.* 3, 1270–1295.
- Sarantis, P., Koustas, E., Papadimitropoulou, A., Papavassiliou, A.G., Karamouzis, M. V., 2020. Pancreatic ductal adenocarcinoma: Treatment hurdles, tumor microenvironment and immunotherapy. *World J. Gastrointest Oncol.* 12, 173–181. <https://doi.org/10.4251/wjgo.v12.i2.173>.
- Savjani, K.T., Gajjar, A.K., Savjani, J.K., 2012. Drug solubility: importance and enhancement techniques. *ISRN Pharm.* 195727. <https://doi.org/10.5402/2012/195727>.
- Sharma, P., Allison, J.P., 2015. Immune checkpoint targeting in cancer therapy: toward combination strategies with curative potential. *Cell* 16, 205–214.
- Takahashi, S., 2018. Molecular functions of SIRP α and its role in cancer. *Biomed. Rep.* 9, 3–7. <https://doi.org/10.3892/br.2018.1102>.
- Uzzaman, M., Mahmud, T., 2020. Structural modification of aspirin to design a new potential cyclooxygenase (COX-2) inhibitors. *Silico Pharmacol.* 8, 1.
- Walum, E., 1998. Acute oral toxicity. *Environ. Health Perspect.* 106 (2), 497–503.
- Yang, S., 2010. Pharmacophore modeling and applications in drug discovery: challenges and recent advances. *Drug Discov. Today* 15, 444–451.
- Yang, Y., 2015. Cancer immunotherapy: harnessing the immune system to battle cancer. *J. Clin. Invest.* 125 (9), 3335–3337.
- Yao, C., Li, G., Cai, M., Qian, Y., Wang, L., Xiao, L., Thaiss, F., Shi, B., 2017. Prostate cancer down-regulated SIRP- α modulates apoptosis and proliferation through p38-MAPK/NF- κ B/COX-2 signaling. *Oncol. Lett.* 13, 4995–5001.
- Zola, H., Swart, B., Nicholson, I., Voss, E., 2020. In: *Leukocyte and Stromal Cell Molecules: The CD Markers*. Wiley, New Jersey, p. 591.